Safe to Fly? Real-Time Flight Mission Feasibility Assessment for Drone Package Delivery Operations

Abenezer Taye **□**

Mechanical and Aerospace Engineering Department, School of Engineering and Applied Science, George Washington University, Washington DC, USA

Austin Coursey □ □

Institute for Software Integrated Systems, Vanderbilt University, Nashville, TN, USA

Marcos Quinones-Grueiro □

Institute for Software Integrated Systems, Vanderbilt University, Nashville, TN, USA

Chao Hu ⊠

School of Mechanical, Aerospace, and Manufacturing Engineering, University of Connecticut, Storrs, CT, USA

Gautam Biswas □

Institute for Software Integrated Systems, Vanderbilt University, Nashville, TN, USA

Peng Wei **□ 0**

Mechanical and Aerospace Engineering Department, School of Engineering and Applied Science, George Washington University, Washington DC, USA

— Abstract -

Ensuring flight safety for small unmanned aerial systems (sUAS) requires continuous in-flight monitoring and decision-making, as unexpected events can alter power consumption and deplete battery energy faster than anticipated. Such events may result in insufficient battery capacity to complete a mission, thereby compromising flight safety. In this paper, we present an online feasibility assessment and contingency management framework that continuously monitors the aircraft's battery state and the energy required to complete the flight in real-time, which enables informed decision-making to enhance flight safety. The framework consists of two main components: power consumption prediction and battery voltage trajectory prediction. The power consumption prediction is conducted using a model that is based on momentum theory, while the voltage trajectory prediction is performed using a Neural Ordinary Differential Equation (Neural ODE)-based datadriven model. By integrating these two components, the framework evaluates the feasibility of a flight mission in real time and determines whether to proceed with the mission or initiate rerouting. We evaluate the framework's performance in a drone delivery scenario in the Dallas-Fort Worth (DFW) area, where the aircraft encounters an unexpected energy depletion event mid-flight. The proposed framework is tasked with assessing the feasibility of completing the mission and, if necessary, rerouting the aircraft for an emergency landing. The results demonstrate that the framework accurately and efficiently detects energy insufficiencies in real-time and re-routes the aircraft to a predefined emergency landing site.

2012 ACM Subject Classification Computing methodologies \rightarrow Control methods; Computing methodologies \rightarrow Model development and analysis

Keywords and phrases Battery Modeling, Neural ODE, Unmanned Aerial Vehicles

Digital Object Identifier 10.4230/OASIcs.DX.2025.8

Funding This work was supported by NASA award #80NSSC21M0087-21-S06.

1 Introduction

1.1 Motivation

Drone package delivery using small unmanned aerial systems (sUAS) is rapidly advancing and nearing widespread implementation. The FAA recently granted approval for companies such as Zipline and Wing Aviation to operate commercial drones in the Dallas-Fort Worth (DFW) area without requiring visual observers, enabling beyond-visual-line-of-sight (BVLOS) operations [11, 12, 16]. This historic authorization represents a significant shift in the regulatory landscape, paving the way for the safe and routine integration of drone deliveries into the national airspace.

Despite these advancements, ensuring the safety of drone delivery operations remains a critical challenge, particularly due to various operational hazards [24]. Among these, hazards related to aircraft components pose a significant risk to the reliability of advanced air mobility (AAM) operations such as drone package delivery. In this work, we specifically focus on one such hazard, which is the risk of insufficient battery capacity to complete a flight mission.

Due to the dynamic and uncertain nature of flight operations, even if pre-departure feasibility assessments account for all known factors, unexpected events during flight can still lead to insufficient battery energy. Various operational factors that happen during flight can influence the power consumption of the aircraft and deplete the battery energy faster than anticipated. For example, a mid-flight incident such as a bird strike may damage a propeller, reducing thrust efficiency and increasing power demand [9]. Similarly, if the electronic speed controller (ESC) or battery overheats beyond a safe threshold, the system may impose a speed restriction [13], limiting the aircraft's operational envelope and requiring rerouting to the nearest landing site.

To mitigate these risks and enhance flight safety, we propose a real-time flight mission monitoring scheme that continuously evaluates the feasibility of a package delivery mission based on the available battery energy. The intended operation of this framework in a real-world drone package delivery scenario is illustrated in Figure 1. The monitoring system is activated immediately after takeoff and periodically assesses whether the mission remains feasible. This enables timely adjustments, such as rerouting to a nearby warehouse or an emergency landing site, to ensure safe operation throughout the flight until the aircraft reaches its destination.

1.2 Related Work

The two areas related to our overall problem are battery state prediction and battery feasibility-based flight planning. Here we summarize the previous works related to these two areas.

1.2.1 Battery State Prediction

Existing battery state prediction methods can be broadly categorized into two approaches: model-based and data-driven methods. Model-based approaches rely on physical models of the battery to predict key states, primarily future trajectories of terminal voltage and state of charge (SoC). These methods typically use either equivalent circuit models or electrochemical-based models, combined with estimators, to forecast battery states over time.

Equivalent circuit models represent the battery's internal dynamics using electrical components such as resistors and capacitors. Common models include the Rint model, the RC model, and the Thévenin model [14]. These models simplify the battery's behavior but

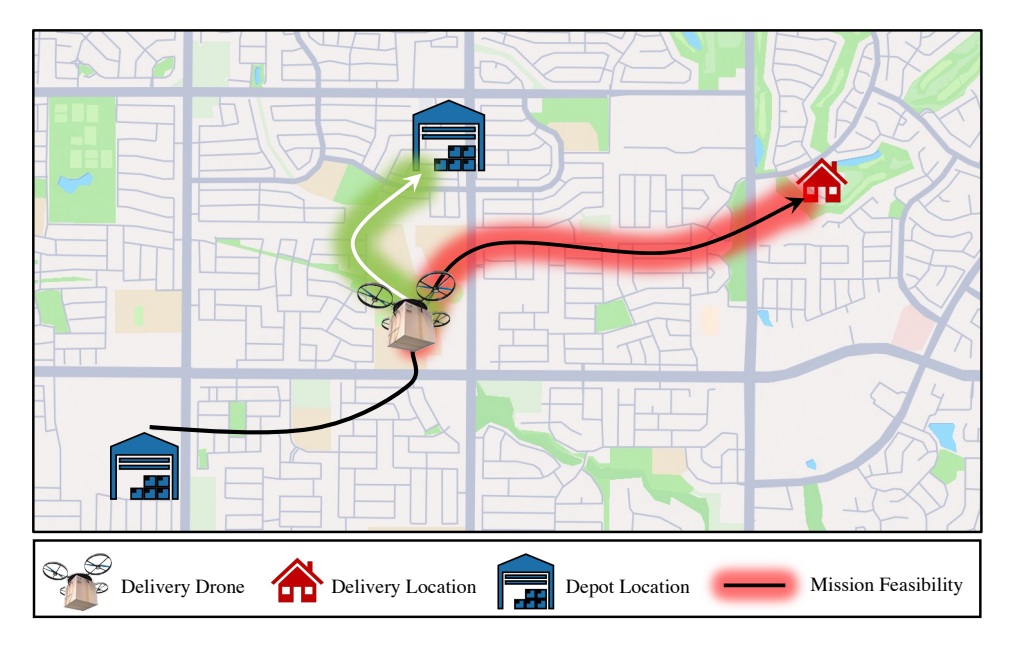


Figure 1 Schematic diagram representation of the feasibility assessment procedure.

still require parameter estimation and state estimation techniques for accurate predictions. In contrast, electrochemical-based models simulate the battery's internal chemistry using porous electrode theory [15] and describe its dynamics through partial differential equations (PDEs). There are multiple versions of these models, varying in complexity depending on the target application, with the most widely used being [8] and [10]. While model-based methods offer high accuracy and interpretability, they require simulating complex, nonlinear battery models, making them computationally expensive and impractical for real-time in-flight applications.

To address this limitation, data-driven approaches have been developed. These methods use machine learning techniques to predict battery states with reduced computational cost. Among the most common are long short-term memory (LSTM) networks [5], support vector machines (SVM) [18], and fuzzy inference systems (FIS) [17]. Data-driven approaches are more computationally efficient [3], making them suitable for real-time applications such as in-flight battery state prediction. However, their accuracy tends to degrade as the prediction horizon increases, limiting their reliability for long-term planning applications.

1.2.2 Battery Feasibility Based Flight Planning

The proposed framework aims to perform online battery state prediction for sUAS operations and assess mission feasibility. Several studies have explored similar goals. For instance, Shibl et al. [22] developed a battery management system for sUAS that employs deep neural networks (DNN) and LSTM networks to predict the SoC and the state of health (SoH). This system enhances battery monitoring and aids in mission planning based on the current battery state. Similarly, [4] proposed a method for assessing mission feasibility by considering battery performance and planning optimal routes to ensure successful mission completion. In another study, Shi et al. [20] introduced a cloud-based framework for the co-estimation of SoC and SoH, leveraging transformer-based deep learning techniques to provide accurate and real-time battery state predictions. Additionally, [21] explored a risk-aware approach for unmanned aerial vehicle and unmanned ground vehicle rendezvous planning using a chance-

constrained Markov Decision Process. Their method accounts for the stochastic nature of energy consumption and optimizes rendezvous points to enhance mission feasibility and safety. Furthermore, Choudhry et al. [7] developed a deep energy model utilizing Temporal Convolutional Networks to predict energy consumption. They introduced a Conditional Value-at-Risk (CVaR) metric to assess the risk of battery depletion during flights, providing a framework for risk-aware mission planning and feasibility assessment.

However, none of these studies approach battery feasibility-based flight planning from the perspective of forecasting the future voltage trajectory. In contrast, our framework introduces a two-stage pipeline that first predicts the power consumption profile of the aircraft for the planned mission and then leverages a data-driven battery model to forecast the corresponding voltage trajectory. This approach enables a more realistic and forward-looking assessment of mission feasibility, unlike prior methods that rely solely on the current battery state or coarse approximations of future energy demands.

2 Problem Formulation

Ensuring the real-time feasibility of flight missions is critical for safe and reliable operations, particularly in applications such as package delivery. The framework proposed in this paper periodically assesses battery feasibility during flight to determine whether the aircraft can successfully reach its destination or if it needs to reroute to an alternate landing site. This section outlines the formulations of the two key components of the feasibility assessment framework – the aircraft model and the battery model – and provides a formal description of the problem addressed in this work.

2.1 Aircraft Model

The aircraft operates in a three-dimensional environment with latitude, longitude, and altitude. The specific aircraft model considered in this paper is an octo-rotor, whose detailed dynamics is provided in [1]. For brevity, we summarize the aircraft dynamics here. At any time t, the aircraft's state in inertial space is represented as $\mathbf{x}_t \in \mathbb{R}^3$, and its evolution follows the system dynamics:

$$\dot{\zeta}_t = f(\zeta_t, u_t),\tag{1}$$

where $f: \mathbb{R}^n \times \mathbb{R} \to \mathbb{R}^n$ is a continuous function. The vector ζ represents the aircraft's states, including its position (x, y, z), velocities $(\dot{x}, \dot{y}, \dot{z})$, angular positions $[\phi, \theta, \psi]$, and angular velocities [p, q, r]. The control input u_t ensures that the aircraft follows a predefined sequence of waypoints from the initial to the final destination.

2.2 Battery Model

The battery model utilized in this study is an electrochemical model of lithium-ion batteries, as described in [8], which are a popular choice for powering unmanned aerial vehicles. In this model, the battery's current draw, denoted by I_b , serves as the input, while the battery voltage V_b , temperature T_b , and state of charge (SoC) represent the system states. The battery dynamics are governed by the following system equation:

$$\dot{\boldsymbol{\xi}}_t = g(\boldsymbol{\xi}_t, I_b),\tag{2}$$

where $g: \mathbb{R}^m \times \mathbb{R} \to \mathbb{R}^m$ is a continuous function. The state vector $\boldsymbol{\xi}$ represents the battery's internal states.

2.3 Problem Description

Consider an aircraft whose airframe and battery dynamics are given by Equation 1 and 2, respectively. The aircraft is assigned to deliver a package from an initial warehouse location $\mathbf{x}_w = (x_w, y_w, z_w)$ to a designated delivery site $\mathbf{x}_d = (x_d, y_d, z_d)$. Once the aircraft completes takeoff, the framework presented in this paper needs to perform a periodic feasibility check every τ seconds to ensure that the mission remains viable under real-time aircraft and environmental conditions. At each reassessment step, where \mathbf{x}_t represents the position of the aircraft at the time of feasibility assessment, the condition for mission success is evaluated using:

$$V_{\text{success}}(t \mid \mathbf{x}_t) \ge V_{\text{thresh}}, \quad \forall t \in [t, t+T].$$
 (3)

If the battery voltage trajectory is greater than or equal to a predefined feasibility voltage threshold ($V_{\rm thresh}$) value, the aircraft continues its flight. However, if at any point in time, the battery voltage drops below the threshold, the aircraft must reroute to the nearest warehouse or designated emergency landing site.

3 Method

To address the problem described in the previous section, we propose the framework shown in Figure 2, where, at each decision-making step, three major tasks are performed: 1) power consumption prediction, 2) battery voltage and SoC prediction, and 3) feasibility assessment and decision making. The remainder of this section discusses these three major tasks of the framework in detail.

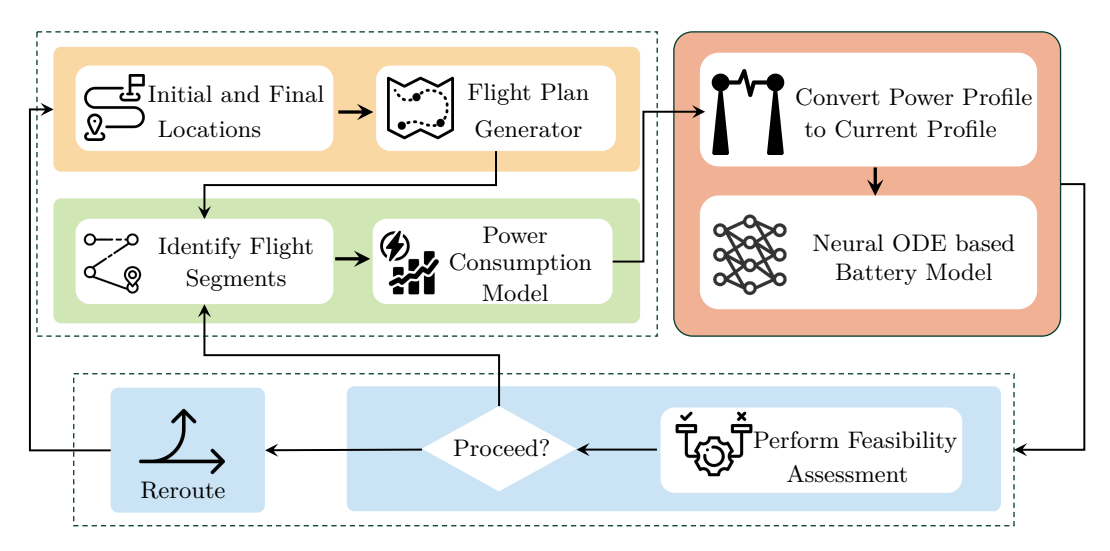


Figure 2 Schematic diagram of the feasibility assessment procedure.

3.1 Power Profile Prediction

Accurate prediction of power consumption for a future flight trajectory is critical for assessing the feasibility of a mission. The proposed framework predicts the power consumption of a future flight trajectory using the following procedure. First, a flight plan is generated for the remaining flight using the initial and final locations. This flight plan comprises waypoints

between these initial and final locations along with the velocity profile of the aircraft. Next, the framework identifies distinct flight segments – such as takeoff, cruise, and landing – and computes the power consumption and flight duration for each flight segment using the power consumption model which is discussed in the following subsection.

3.1.1 Aircraft Power Consumption Model

To determine the power required for future flight operations, the ideal approach would be to simulate the detailed aircraft dynamic model and collect the power required for future flight duration. However, since the detailed aircraft dynamic model is complex and highly nonlinear, doing so is computationally expensive. To address this challenge, we adopt a power consumption model for rotary-wing aircraft from [23]. This model is based on momentum theory and incorporates aerodynamic equations for each flight maneuver including, climb, hover, horizontal flight, and descent.

$$P_{\text{hover}} = \frac{W^{\frac{3}{2}}}{\eta_h \cdot \sqrt{2\rho A_t}},\tag{4}$$

$$P_{\text{climb}} = \frac{W}{\eta_c} \left(\frac{V_c}{2} + \sqrt{\frac{V_c^2}{4} + \frac{W}{2\rho A_t}} \right), \tag{5}$$

$$P_{\text{descent}} = \frac{W}{\eta_c} \left(\frac{-V_d}{2} + \sqrt{\frac{V_d^2}{4} + \frac{W}{2\rho A_t}} \right),\tag{6}$$

where V_c and V_d are vertical climb speed and vertical descent speed values, respectively. In addition, η is the efficiency factor of the propulsion system, ρ is the air density, W is the total weight of the aircraft, and A_t is the sum of the n-disc actuator areas. In addition, the instantaneous power for horizontal flight is given as:

$$P_{\text{horizontal}} = \frac{W}{\eta_{\text{hor}}} \left(V_{\text{hor}} \sin(\alpha_v) + v_{\text{hor}} \right), \tag{7}$$

where α_v is the angle of attack and η_{hor} and the horizontal efficiency. In addition, the induced velocity in horizontal flight v_{hor} , is given by:

$$v_{\text{hor}} = \sqrt{-\frac{V_{\text{hor}}^2}{2} + \sqrt{\frac{V_{\text{hor}}^4}{4} + (\frac{W}{2\rho A_t})^2}}.$$
 (8)

All the aircraft-related parameters mentioned in the equations above are given in Table 1.

3.1.2 Flight Duration Estimation

The aircraft power consumption model outlined above provides the instantaneous power required by the aircraft during a given timestamp in a specific flight phase. However, to predict the power profile for each flight segment, we must also determine the duration of each segment. Here, we discuss the approach used to estimate the flight duration of each flight segment. During a climb or descent, the aircraft changes altitude at a constant speed, and the total time required to reach the desired attitude is given by:

$$T_{\text{climb/descend},i} = \frac{h_{i+1} - h_i}{V_{\text{climb/descend}}},$$
 (9)

Aircraft Parameters		Battery Parameters		
ρ	Air density (1.225 kg/m^3)	R_{int}	Internal resistance (0.05 Ω)	
A_t	Rotor disk area (1.31 $\mathrm{m}^2)$	η	Battery efficiency (0.95)	
W	Aircraft weight (10 kg)	C_n	Nominal capacity (22000 mAh)	
η_c	Climb efficiency (0.85)	k_0	Open-circuit voltage constant (22.83)	
α_v	Horizontal drag coefficient (0.25)	k_1	Open-circuit voltage constant (0.39)	
η_d	Descent efficiency (0.75)	k_2	Open-circuit voltage constant (-0.78)	
$\eta_{ m hor}$	Horizontal efficiency (0.88)	$V_{ m thresh}$	Battery voltage threshold (18 V)	

Table 1 Aircraft- and battery-related parameters.

where $h_{i+1} - h_i$ represents the altitude change and V_{climb} or (V_{descend}) is the predefined climb (or descent) speed. Similarly, once the aircraft reaches cruising altitude, the aircraft moves with a constant horizontal velocity. The cruise time for a given segment is computed as:

$$T_{\text{cruise},i} = \frac{d_i}{V_{\text{cruise}}},$$
 (10)

where d_i is the horizontal distance of the segment and V_{cruise} is the predefined cruise speed. Finally, the overall flight power profile is obtained by concatenating the power profiles for the climb, cruise, and descent segments, each computed over its respective flight duration:

$$P_{\text{flight}} = [P_{\text{climb}}, P_{\text{cruise}}, P_{\text{descend}}]. \tag{11}$$

3.2 Power to Current Conversion

After predicting the power profile for the entire flight, we need to convert it into a current profile to use as input for our Neural ODE-based battery model. However, this conversion is not straightforward, as both voltage and current are unknown in our problem setting. To address this, we adopt the Rint-based equivalent circuit model [14]. This model represents the battery as an ideal voltage source in series with a single resistor and is described by the following equation:

$$V(t) = V_{\rm oc}(t) - I(t)R_{\rm int},\tag{12}$$

where V(t) is the battery voltage, $V_{\text{oc}}(t)$ is the open circuit voltage, and R_{int} represents the internal resistance of the battery. By rewriting this equation using the relationship $P(t) = V(t) \cdot I(t)$, we obtain the following quadratic equation:

$$I(t)^{2}R_{\text{int}} - V_{\text{oc}}(t)I(t) + P(t) = 0.$$
(13)

In the above equation, $V_{oc}(t)$ is determined from the OCV-SoC curve of the battery, assuming the SoC of the battery at a given time is known. In this study, we use the Nernst model to represent the OCV-SoC relationship, which is commonly applied to Li-ion and Li-Po batteries:

$$V_{\rm oc}({\rm SoC}) = k_0 + k_1 \ln({\rm SoC}) + k_2 \ln(1 - {\rm SoC}),$$
 (14)

where the parameters $k_0 = 22.83$, $k_1 = 0.39$, and $k_2 = -0.78$ are obtained by fitting battery data [2]. Figure 3 shows the fitted OCV-SoC curve. Once the SoC is determined, this curve is used to obtain the corresponding open-circuit voltage of the battery. The

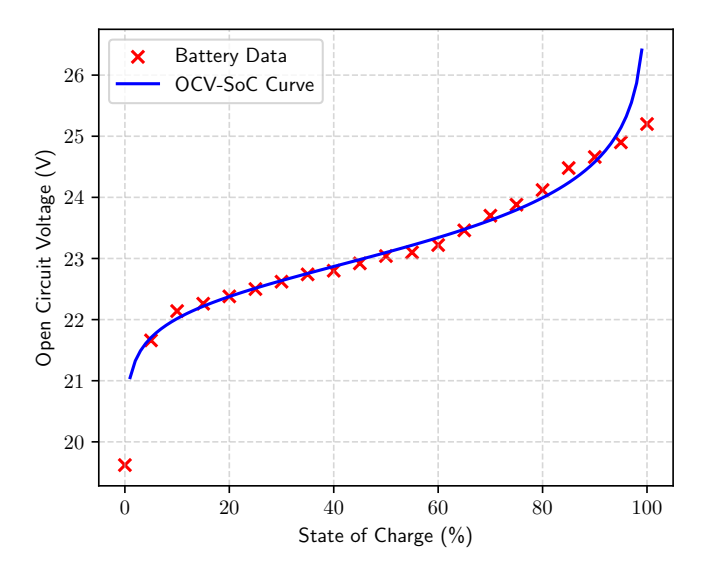


Figure 3 Fitted SoC vs OCV Curve for the 6S1P 22Ah Battery.

SoC at any given time is estimated using coulomb counting (also known as Ampere-Hour integration), which estimates the SoC by measuring the amount of charge and discharge using the following equation:

$$SoC(t) = SoC(t_0) - \frac{\eta}{C_n} \int_{t_0}^t I(t)dt, \tag{15}$$

where $SoC(t_0)$ is the initial state of charge, η represents the coulumbic efficiency, C_n represents the battery capacity or rated capacity, and I(t) is the instantaneous current discharged from the battery.

Finally, the derived current profile, along with the current battery voltage value and the future flight time horizon, is fed into the data-driven battery model. This learning-based model predicts the voltage and SoC evolution along the anticipated flight trajectory. A detailed description of the learning-based battery modeling is provided in Section 4.

3.3 Feasibility Assessment and Decision Making

After computing the power required to complete the remaining trajectory and predicting the battery's voltage trajectory, we assess mission success using the criterion provided in Equation 3. At each reassessment step, if the predicted voltage trajectory remains greater than or equal to the predefined threshold $V_{\rm thresh}$ throughout the entire prediction horizon, the aircraft continues its flight as planned. However, if the predicted voltage falls below the threshold at any point, the aircraft must reroute to the nearest warehouse or designated emergency landing site. The closest alternate landing site is determined by:

$$\mathbf{x}_{e}^{*} = \arg\min_{\mathbf{x}_{e} \in \mathcal{E}} d(\mathbf{x}_{t}, \mathbf{x}_{e}), \tag{16}$$

where \mathcal{E} represents the set of predefined emergency landing sites, and $d(\mathbf{x}(t), \mathbf{x}_e)$ is the distance between the current position of the aircraft and each landing site. Once a new landing site is identified, the aircraft adjusts its trajectory accordingly and proceeds toward the new landing site. A feasibility assessment is then conducted for the updated trajectory to ensure that the aircraft can safely reach the new destination.

Algorithm 1 Power-to-Current Conversion Process.

```
Procedure Power-to-CurrentConversion():

Input: Power profile P(t), Battery parameters (R_{\text{int}}, \eta, C_n, k_0, k_1, \text{ and } k_2)

Output: Current profile I(t)

for each timestep t do

Compute open circuit voltage (OCV) from SoC using equation 14

V_{\text{oc}}(t) \leftarrow k_0 + k_1 \ln(\text{SoC}(t)) + k_2 \ln(1 - \text{SoC}(t))

Solve quadratic equation 13

I(t) \leftarrow \frac{-V_{\text{oc}}(t) + \sqrt{V_{\text{oc}}(t)^2 - 4R_{\text{int}}P(t)}}{2R_{\text{int}}}

Update SoC using Coulomb counting

SoC(t + \Delta t) \leftarrow SoC(t) - \frac{\eta}{C_n}I(t)\Delta t

End of operation
```

4 Battery Modeling

To enable accurate, data-driven modeling of battery voltage under future current loads, we implemented a Neural Ordinary Differential Equation (Neural ODE) approach [6]. Neural ODEs generalize traditional neural networks by replacing discrete layer-wise transformations with a continuous-time formulation, where the hidden state h(t) evolves according to a learned differential equation:

$$\frac{dh}{dt} = f(h(t), t; \theta) \tag{17}$$

Here, f is a neural network parameterized by θ that defines the dynamics of the hidden state over time. In the context of battery modeling, the input current profile and initial voltage are encoded into the initial hidden state h(0), which is then evolved forward in time using an ODE solver. At each time step, the evolving hidden state is used to predict the corresponding battery voltage. This framework naturally supports irregular time sampling and produces smooth, physically coherent predictions, making it particularly effective for capturing the dynamics of battery behavior under variable loads.

In this section, we describe the procedures followed to develop the Neural-ODE-based battery model. The overall training workflow for the Neural ODE-based battery model is illustrated in the schematic diagram shown in Figure 4. As depicted in the figure, the modeling process includes dataset generation, construction of training and test sets, model training using the training set, and performance evaluation using the test set.

4.1 Dataset Generation

To develop and validate a data-driven battery voltage prediction model, we adopted a data generation procedure designed to capture the dynamic behavior of a lithium-ion battery under diverse load conditions. This procedure integrates a high-fidelity electrochemical battery

Figure 4 Neural ODE-based battery model training processes.

model with a current profile generation mechanism to emulate realistic operational scenarios in drone package delivery missions. The goal is to produce realistic current and voltage profiles that reflect battery performance during flight operations. The data generation approach consists of three main stages: (i) flight mission current profile generation, (ii) simulation of battery voltage, and (iii) dataset construction.

4.1.1 Flight Mission Current Profile Generation

The current profile generation process produces two types of profiles: full-flight mission profiles and mid-flight constant profiles. Full-flight profiles capture both the takeoff and cruise phases of the aircraft operations, where the takeoff phase is characterized by a higher power demand, while the cruise phase exhibits a lower current draw. Mathematically, the generated current profile at time t, denoted as I(t), is defined as:

$$I(t) = \begin{cases} I_{\text{takeoff}}, & 0 \le t < T_{\text{takeoff}} \\ I_{\text{cruise}}, & T_{\text{takeoff}} \le t < T_{\text{total}} \end{cases}$$
(18)

where $I_{\rm takeoff} \sim U(140, 225)$ A and $I_{\rm cruise} \sim U(50, 70)$ A, with U(a, b) denoting a uniform distribution. The takeoff duration, $T_{\rm takeoff}$, is randomly sampled within the range [1, 10] seconds, ensuring variability in the generated profiles. Mid-flight profiles, on the other hand, are created by assigning the initial voltage at various points during a full-flight mission and applying a constant current profile from that point onward. This approach enables the evaluation of battery response under different initial conditions.

4.1.2 Battery Voltage Simulation

To simulate the voltage response corresponding to the generated current profiles, we employ an electrochemical battery model [8]. The simulation procedure involves initializing the battery state, iterating over the generated current profiles, and computing the corresponding voltage response. The resulting dataset consists of 1,000 pairs of current and voltage trajectories and is systematically divided into training and test sets using a 70% - 30% split. Each entry in the dataset comprises the input current trajectory I(t), the corresponding voltage response V(t), and the associated time horizon T. Figure 5 illustrates representative samples from the generated dataset, with current trajectories shown in blue and their corresponding voltage responses in black.

4.2 Neural ODE Training

In this subsection, we provide details on the data preprocessing steps, as well as the architectural and training specifications of our Neural ODE-based battery model.

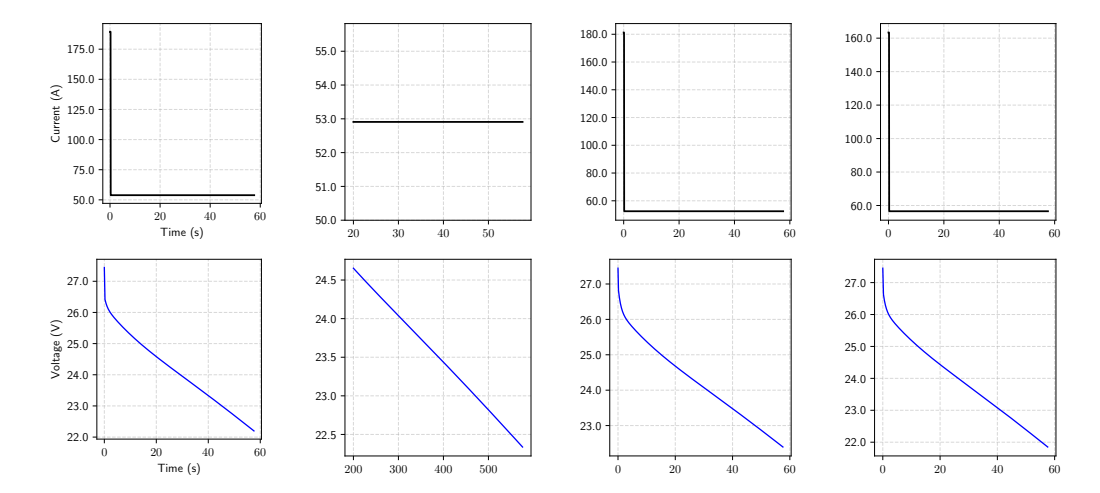


Figure 5 Representative current profiles (top row) and their corresponding voltage responses (bottom row).

4.2.1 Data Preprocessing

To ensure robust generalization across various scales of input data and to mitigate numerical instability during training, the input current and output voltage sequences are standardized using the training dataset's mean and standard deviation. The model operates on normalized time in the range [0, 1] for each sequence.

4.2.2 Neural ODE Model Architecture

Our Neural ODE model consists of two primary components: a neural network-based ODE function and an ODE solver. The ODE function is implemented as a fully connected feedforward neural network with three hidden layers, each employing ReLU activation functions, and outputs the derivative of the voltage. The network takes as input the initial battery voltage, the input current, and the time horizon, enabling it to learn a continuous-time differential equation that governs the voltage dynamics. This learned function is then integrated over time using a fourth-order Runge-Kutta (RK4) solver to generate the battery voltage trajectory. The model is trained using a composite loss function that combines mean squared error (MSE) and root mean squared error (RMSE) between the predicted and ground truth voltage values. After training, the model is evaluated on test current profiles to assess its accuracy in predicting voltage trajectories. The architectural and training hyperparameter details of the model are provided in Tables 2 and 3, respectively. These parameters were identified through a series of empirical experiments, where different configurations were systematically tested to achieve optimal trade-offs between model complexity, training efficiency, and predictive performance.

5 Results and Discussion

5.1 Scenario Description

The scenario designed in this paper to evaluate the performance of the proposed real-time feasibility assessment and contingency management framework involves a drone package delivery operation within the Dallas–Fort Worth (DFW) metropolitan area, as illustrated

Table 2 Architecture of the ODE function.

Layer	# Neurons	Activation
Input	3	_
Layer 1	128	ReLU
Layer 2	128	ReLU
Layer 3	64	ReLU
Output	1	None

Table 3 Training hyperparameters.

Hyperparameter	Value
Optimizer	Adam
Learning Rate	0.001
Batch Size	4
ODE Solver	RK4
Epochs	100

in Figure 6. In this scenario, a single aircraft departs from a designated warehouse located at 33°08′48″N, 96°48′22″W, flying towards an assigned delivery location at 33°09′05″N, 96°47′15″W. We assume all necessary pre-departure feasibility assessments have already been completed, and the mission has been cleared for execution. Once airborne, the online feasibility assessment method developed in this study, which is assumed to run offboard, operates at regular intervals of 5 seconds.

Additionally, to assess the effectiveness of our proposed approach in supporting online decision-making and contingency management, we introduce a realistic in-flight anomaly scenario. In this case, the aircraft experiences an anomaly upon reaching the midpoint of the mission, located at coordinates $33^{\circ}08'56.5''N$, $96^{\circ}47'48.5''W$. Due to thermal stress affecting the electronic speed controller (ESC), the cruise speed must be reduced from the nominal 5 m/s to 3 m/s. This reduction significantly extends the expected flight duration and increases energy consumption, potentially rendering the original flight plan infeasible.

In response, the aircraft must perform a feasibility assessment under the new flight condition and dynamically reroute to one of several predefined emergency landing sites to ensure safety. These alternative landing sites are located at 33°08′40″N, 96°48′12″W; 33°09′04″N, 96°47′45″W; and 33°09′12″N, 96°47′11″W. As shown in Figure 6, these locations are labeled Emergency Landing 1, Emergency Landing 2, and Emergency Landing 3, respectively. This scenario provides a rigorous testbed for evaluating the framework's capability to forecast infeasibility and adapt flight decisions in real time.

5.2 Results

Because our framework conducts the feasibility assessment in two steps – first predicting the power profile and then predicting the battery voltage – we evaluate the accuracy of each step independently. To validate the predicted power profiles, we use the detailed aircraft model presented in [1] as our ground truth. Similarly, for battery voltage performance evaluation, we employ the detailed electrochemical Li-ion battery model described in [8] as the reference. Furthermore, since the online feasibility assessment occurs at fixed time intervals, voltage predictions made at each timestep are visualized using distinct colors, with each color corresponding to the prediction profile generated at a specific feasibility assessment timestep.

5.2.1 Power Consumption Prediction Results

As discussed in Section 5.1, our package delivery scenario involves two main flight phases: one before the mid-flight incident and another after the incident. Before the mid-flight incident, the aircraft is executing the original flight plan which is from the warehouse to the assigned destination (referred to as "Long"). However, once the mid-flight incident is

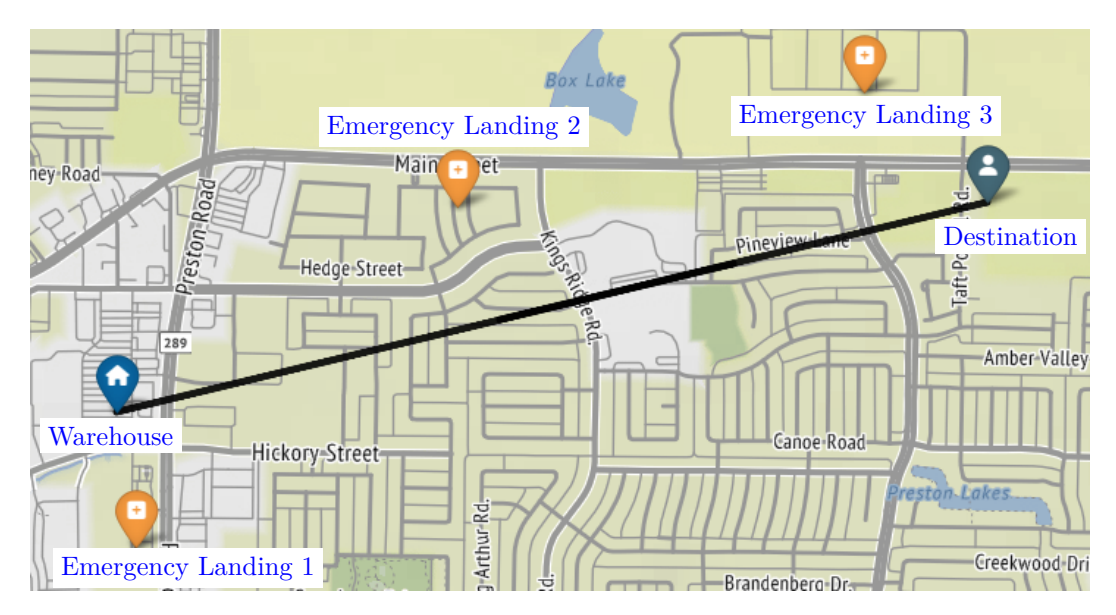


Figure 6 The developed package delivery scenario illustrating the original flight plan, warehouse, destination, and the three emergency landing sites.

identified and the speed change is applied, the aircraft needs to assess the feasibility of the original flight plan with the newly updated speed and if it's not feasible, identify the nearest emergency landing site from the already pre-defined set of locations and fly towards it while still performing the feasibility assessment at every 5 seconds.

Following the mid-flight incident, four alternative flight plans are considered, each corresponding to a potential landing site: the original destination and the three emergency landing sites. These include: (i) the flight plan to the original destination after the incident, which is expected to be infeasible and is labeled "Infeasible"; (ii) the flight plan to the nearest emergency landing site, labeled "Short"; and (iii) the flight plans to the other two emergency landing sites, labeled "EM1" and "EM3", respectively.

Figure 7 presents a comparison between the actual aircraft power consumption profiles and the approximated power profiles for three flight plans: "Long", "Infeasible", and "Short". These approximations are obtained using the method described in Section 3.1. Since the mid-flight incident requiring cruise speed reduction occurs at 288 seconds, the second and third plots show the power profiles only for the remaining flight duration from the moment the speed reduction is applied. Furthermore, the lower three plots in Figure 7 compare the actual current profiles against those derived from the predicted power trajectories using the conversion technique outlined in Section 3.2. This analysis enables a direct evaluation of the prediction pipeline's ability to infer current demands under altered flight conditions.

Because the reliability of our decision-making and contingency management framework heavily depends on the predictive accuracy of the power consumption model and the power-to-current conversion process, we evaluate the performance of these key components in Table 4. The table presents the results of 30 simulation runs for each of all flight plans. For each case, we report the average root mean squared error (RMSE) and mean absolute error (MAE) between the model-based reference approach and the method proposed in this paper. The results demonstrate that the proposed framework is capable of predicting both power and current profiles with reasonable accuracy.

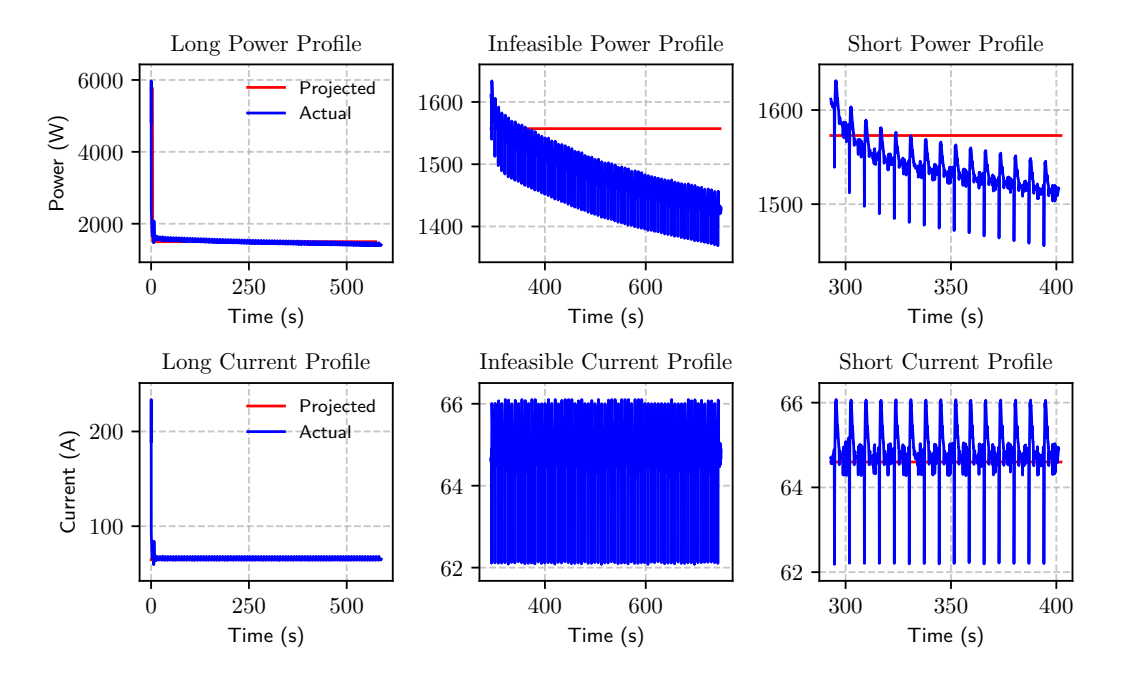


Figure 7 Power and current profiles for the three flight plans (Long, Infeasible, and Short). The top three plots illustrate the power profiles corresponding to each flight plan, while the bottom three plots show the current profiles derived from these power profiles.

5.2.2 Voltage Prediction Results

Once the current profiles for the future flight duration at each timestep are obtained, they are fed into the trained data-driven battery model to predict the corresponding voltage trajectories. Figures 8 and 9 present the predicted voltage trajectories for all flight plans using the Neural-ODE-based approach, alongside the reference battery voltage trajectories generated by simulating the detailed battery model. For each voltage prediction shown in Figures 8 and 9, feasibility assessment is performed at 5-second intervals using the criterion described in Section 1. The minimum voltage threshold for mission feasibility is set at 18 V, meaning the predicted voltage trajectory must remain above this threshold throughout the entire operational time horizon for the mission to be considered safe.

As illustrated in Figure 8, the predicted voltage trajectory for the original flight plan remains above the 18 V threshold at all times and is therefore considered feasible – until the mid-flight incident occurs. However, as shown in the middle plot of Figure 8, once the incident triggers a reduction in cruise speed to 3 m/s, the voltage trajectory violates the threshold at approximately 680 seconds. This indicates that the aircraft can no longer safely complete its flight to the assigned destination. Consequently, the mission is rerouted to the emergency landing site, and feasibility is re-evaluated using the current profile for the short flight plan with the Neural-ODE-based battery model. The result, shown in the final plot of Figure 8, demonstrates that the revised mission remains feasible under the updated flight conditions, thereby ensuring the safety of the aircraft.

To provide a more comprehensive understanding of the mid-flight incident and the rationale behind the chosen contingency plan, Figure 9 presents the voltage predictions for the two alternative flight plans directed toward the other emergency landing sites ("EM1" and

Profile	Error Type	Long	Infeasible	Short	EM1	EM3
Power (W)	RMSE	295.01	83.82	39.41	75.36	75.37
rower (w)	MAE	68.80	74.84	35.06	66.89	66.80
Cumant (A)	RMSE	3.76	0.63	0.60	0.63	0.63
Current (A)	MAE	0.94	0.39	0.38	0.39	0.39

Table 4 Comparison of prediction accuracy (RMSE and MAE) for power and current profiles across all flight plans: Long, Infeasible, Short, EM1, and EM3.

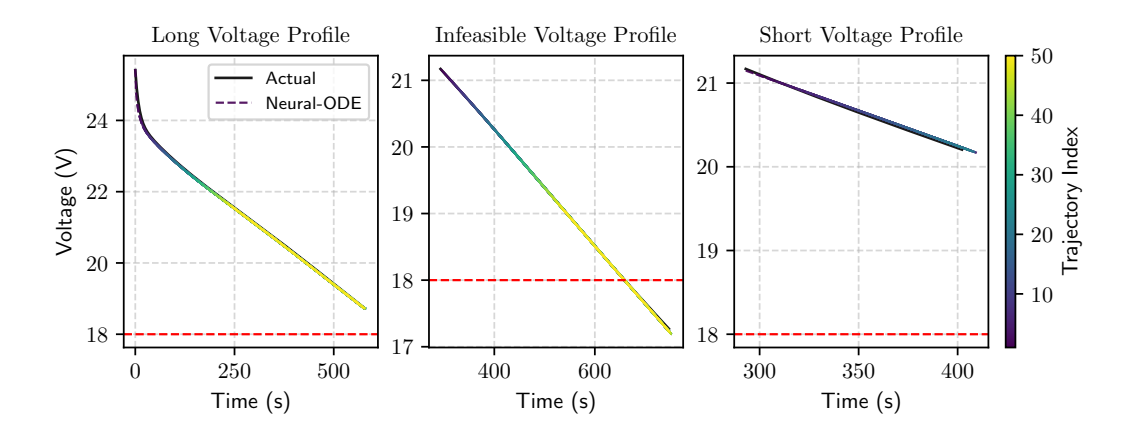


Figure 8 Voltage predictions for the three flight plans (Long, Infeasible, and Short), performed at 5-second intervals. Each voltage profile corresponds to a specific prediction index, representing the voltage trajectory forecasted at a given feasibility assessment timestep.

"EM3"). The results clearly demonstrate that both of these trajectories become infeasible, as the predicted battery voltage drops below the minimum operational threshold. This confirms the validity of the selected rerouting strategy to the nearest emergency landing site ("Short").

Furthermore, Figure 10 offers a spatial visualization of the voltage predictions overlaid on the mission map. In this figure, each flight plan is illustrated using a heatmap that encodes predicted battery voltage along the flight trajectory. As shown, the battery begins fully charged at the warehouse, but following the mid-flight incident, the voltage predictions for all flight plans – except for the one directed to Emergency Landing 2 – fall below the critical threshold of 18 V at some point along the trajectory. This spatial voltage analysis further reinforces the feasibility of the re-routing decision and highlights the framework's efficacy in supporting real-time contingency management.

To evaluate the performance of the Neural-ODE-based battery model used for online feasibility assessment, we examine both its prediction accuracy and computational efficiency. For benchmarking purposes, we developed a physics-informed neural network (PINN) [19] based battery model, which is considered a state-of-the-art approach for learning battery dynamics. The PINN model implemented in this study combines a long short-term memory (LSTM) network with an equivalent circuit-based battery model adopted from [14]. This approach enhances the predictive capabilities of the data-driven LSTM by embedding physical laws – specifically, the voltage-current relationships described by the equivalent circuit – directly into the training process. Rather than relying solely on data, the PINN

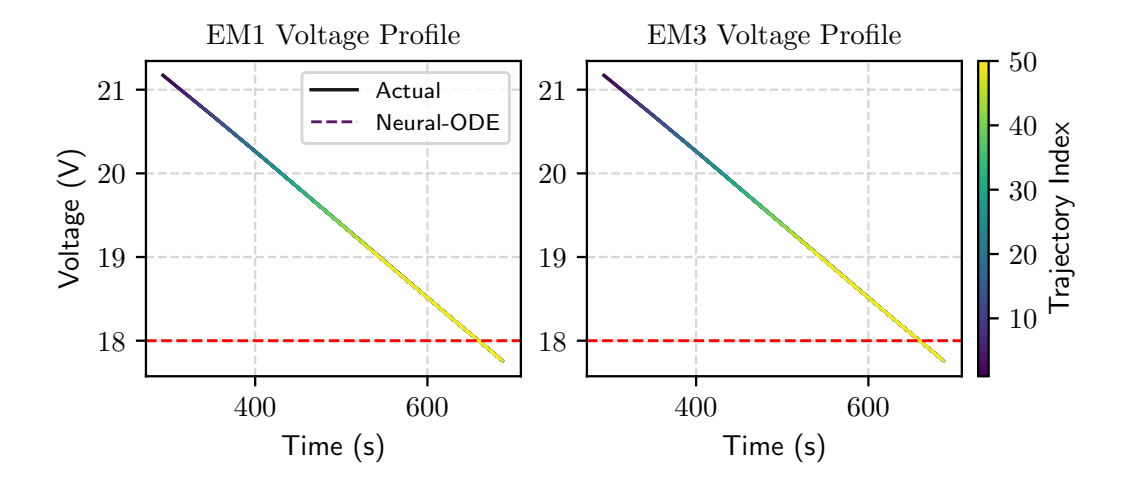


Figure 9 Voltage predictions for flight plans going to emergency landing 1 and emergency landing 3. Each voltage profile corresponds to a specific prediction index, representing the voltage trajectory forecasted at a given feasibility assessment timestep.



Figure 10 Spatial visualization of voltage predictions along each flight trajectory. Arrows indicate the aircraft's flight direction before and after the mid-flight incident.

minimizes a composite loss function that penalizes both data mismatch and violations of the governing physical equations. This integration of domain knowledge improves model generalization, increases robustness to noise, and enables physically consistent predictions even in extrapolated conditions.

Figure 11 presents a comparison between the Neural-ODE and PINN-based approaches for the three flight plans. As shown in the left plot, the Neural-ODE-based model consistently outperforms the PINN model in terms of prediction accuracy across all predictions. These differences in prediction accuracy have important implications for the safety and efficiency of aircraft operations. Specifically, for the long flight plan, the PINN-based feasibility

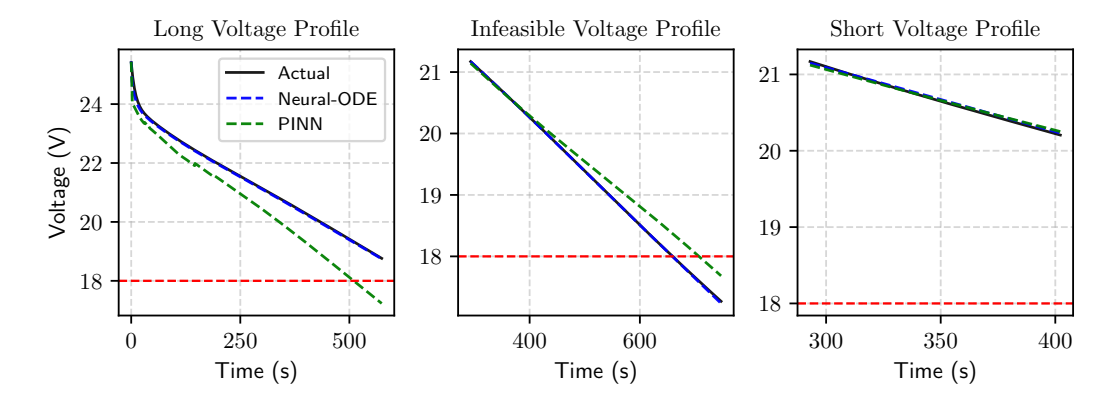


Figure 11 Performance comparison between the Neural-ODE and PINN-based battery models relative to the actual voltage trajectories across all three flight plans.

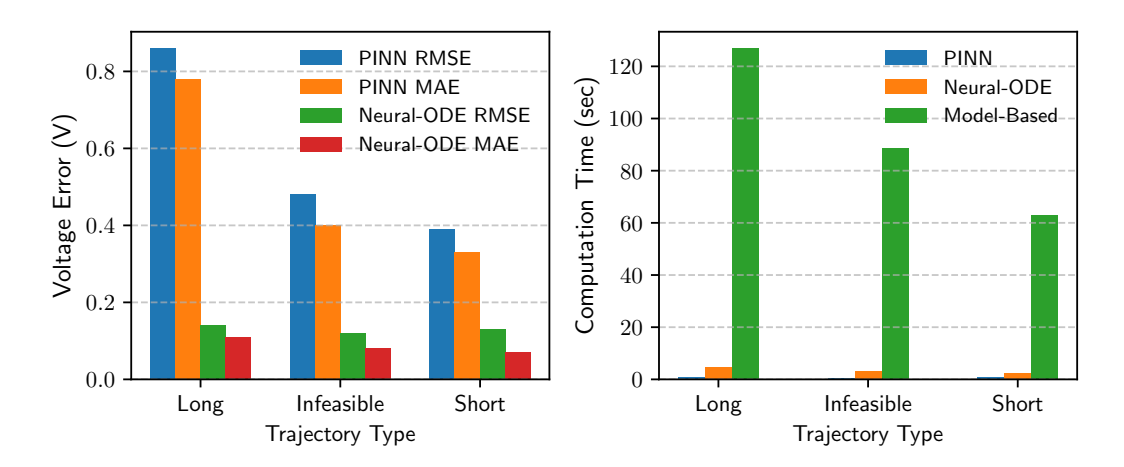


Figure 12 Comparison of accuracy and computational cost between the Neural-ODE and PINN-based battery models. The left plot shows prediction accuracy relative to the ground truth voltage trajectories for all three flight plans, while the right plot presents the average computational time required for feasibility assessments.

assessment would incorrectly classify the mission as infeasible due to its prediction inaccuracies. Conversely, in the case of the infeasible flight plan, the PINN model would fail to detect the voltage threshold violation, potentially resulting in an unsafe decision to proceed with the mission.

In addition to accuracy, computational efficiency is a critical factor, as the framework is intended for real-time use during flight, where computational resources are limited. To assess this, the right plot in Figure 12 shows the average computational time required to perform feasibility assessments for the three flight plans (Long, Infeasible, and Short), comparing the model-based approach with the proposed Neural-ODE approach. All experiments were conducted on a 3.20 GHz Intel Xeon(R) CPU with 125.4 GB of RAM. The results show that the proposed approach is approximately 36 times faster than the model-based method in the long flight plan case, with a maximum computation time of 3.76 seconds. This demonstrates that the proposed framework is well-suited for in-flight operation, where feasibility assessments must be performed every 5 seconds.

5.3 **Discussion and Lessons Learned**

This study provides key insights that may guide future researchers in developing real-time flight mission feasibility assessment frameworks. By implementing and evaluating our proposed framework in a realistic drone package delivery scenario, we identified several important observations and lessons learned.

- Decoupling feasibility assessment into power consumption and voltage trajectory prediction enhances flexibility and accuracy. The proposed framework decomposes the feasibility assessment process into two stages: power consumption prediction and voltage trajectory prediction. This separation allows greater flexibility in selecting and improving prediction models, leading to higher accuracy and computational efficiency. As demonstrated in the results, this structured approach achieves both prediction accuracy and computational efficiency required for real-time feasibility assessment.
- The choice of the power consumption model significantly impacts performance. The efficacy of feasibility assessment is highly dependent on the accuracy of the power consumption model. In this work, we adopted a momentum theory-based power consumption model for multirotor aircraft and fine-tuned it using experimental data. The decision to develop or adopt a power consumption model should consider key factors such as accuracy requirements, computational efficiency, and environmental conditions (e.g., wind effects). Selecting an appropriate model is crucial for ensuring reliable power predictions.
- Power-to-current conversion must account for battery behavior. Given the extended prediction horizon required in our study (approximately 10 minutes), powerto-current conversion must incorporate battery dynamics. Our approach utilizes an open-circuit voltage (OCV) vs state of charge (SoC) relationship modeled using the Nernst equation, combined with Coulomb counting, to achieve an accurate conversion. Careful modeling of this process is essential to maintain prediction reliability over longduration flights.
- The choice of battery modeling technique affects prediction accuracy. Given that battery behavior is inherently governed by differential equations, we adopted a Neural ODE-based model to learn the underlying battery dynamics. To benchmark its performance, we compared it against other time-series prediction techniques, including physics-informed neural networks (PINNs), which combine long short-term memory (LSTM) networks with an equivalent circuit-based battery model. Our results indicate that the Neural ODE-based approach more accurately captures battery voltage trajectories, making it a promising candidate for the feasibility assessment of dynamical systems.

Conclusion

In this paper, we address the problem of online flight mission feasibility assessment for sUAS operations. Unexpected in-flight events can introduce significant safety risks if not properly managed. To mitigate these risks, we propose a framework that continuously monitors battery status and makes real-time decisions to prevent energy insufficiency. The framework consists of two main components: power consumption prediction and battery voltage trajectory prediction. Power consumption prediction is performed using a model based on momentum theory, while voltage trajectory prediction leverages a Neural Ordinary Differential Equation (Neural ODE)-based data-driven model. By integrating these two components, the system evaluates mission feasibility in real time and determines whether to continue the flight or initiate rerouting. We evaluate the framework's performance in a drone delivery scenario in the Dallas-Fort Worth (DFW) area, where the aircraft encounters

an unexpected energy depletion event mid-flight. The results show that the framework accurately predicts power profiles and voltage trajectories for the remaining flight duration. Additionally, its computational efficiency makes it feasible for real-time flight monitoring and contingency management. Future work will incorporate additional sources of uncertainty, such as wind disturbances and noise in the battery model, to improve prediction accuracy and decision-making capabilities. We will also extend the battery model to account for degradation and state of health effects.

- References

- 1 Ibrahim Ahmed, Marcos Quinones-Grueiro, and Gautam Biswas. A high-fidelity simulation test-bed for fault-tolerant octo-rotor control using reinforcement learning. In 2022 IEEE/AIAA 41st Digital Avionics Systems Conference (DASC), pages 1–10. IEEE, 2022. doi:10.1109/DASC55683.2022.9925862.
- 2 AMPOW. Lipo voltage chart: Show the relationship of voltage and capacity, 2023. Accessed: 2025-03-06. URL: https://blog.ampow.com/lipo-voltage-chart/.
- 3 Luca Biggio, Tommaso Bendinelli, Chetan Kulkarni, and Olga Fink. Ageing-aware battery discharge prediction with deep learning. *Applied Energy*, 346:121229, 2023.
- 4 Zdeněk Bouček and Miroslav Flídr. Mission planner for uav battery replacement. In 2024 IEEE International Conference on Multisensor Fusion and Integration for Intelligent Systems (MFI), pages 1–6. IEEE, 2024.
- 5 Ephrem Chemali, Phillip J Kollmeyer, Matthias Preindl, Ryan Ahmed, and Ali Emadi. Long short-term memory networks for accurate state-of-charge estimation of li-ion batteries. *IEEE Transactions on Industrial Electronics*, 65(8):6730–6739, 2017. doi:10.1109/TIE.2017. 2787586.
- 6 Ricky TQ Chen, Yulia Rubanova, Jesse Bettencourt, and David K Duvenaud. Neural ordinary differential equations. Advances in neural information processing systems, 31, 2018.
- 7 Arnav Choudhry, Brady Moon, Jay Patrikar, Constantine Samaras, and Sebastian Scherer. Cvar-based flight energy risk assessment for multirotor uavs using a deep energy model. In 2021 IEEE International Conference on Robotics and Automation (ICRA), pages 262–268. IEEE, 2021. doi:10.1109/ICRA48506.2021.9561658.
- 8 Matthew Daigle and Chetan S Kulkarni. Electrochemistry-based battery modeling for prognostics. In *Annual Conference of the PHM Society*, volume 5(1), 2013. doi:10.36001/phmconf. 2013.v5i1.2252.
- 9 Aditya Devta, Isabel C Metz, and Sophie F Armanini. Experimental evaluation of bird strikes in urban air mobility. arXiv preprint arXiv:2308.13022, 2023. doi:10.48550/arXiv.2308.13022.
- Marc Doyle, Thomas F Fuller, and John Newman. Modeling of galvanostatic charge and discharge of the lithium/polymer/insertion cell. *Journal of the Electrochemical society*, 140(6):1526, 1993.
- Federal Aviation Administration. Package delivery by drone (part 135), 2023. Accessed: 2024-10-19. URL: https://www.faa.gov/uas/advanced_operations/package_delivery_drone.
- Federal Aviation Administration. Faa makes drone history in dallas area, 2024. Accessed: 2024-10-19. URL: https://www.faa.gov/newsroom/faa-makes-drone-history-dallas-area.
- 13 George E Gorospe Jr, Chetan S Kulkarni, Edward Hogge, Andrew Hsu, and Natalie Ownby. A study of the degradation of electronic speed controllers for brushless dc motors. In Asia Pacific Conference of the Prognostics and Health Management Society 2017, volume ARC-E-DAA-TN42858, 2017.
- Hongwen He, Rui Xiong, and Jinxin Fan. Evaluation of lithium-ion battery equivalent circuit models for state of charge estimation by an experimental approach. *energies*, 4(4):582–598, 2011.

- Dickson NT How, MA Hannan, MS Hossain Lipu, and Pin Jern Ker. State of charge estimation for lithium-ion batteries using model-based and data-driven methods: A review. *Ieee Access*, 7:136116–136136, 2019. doi:10.1109/ACCESS.2019.2942213.
- Yves Le Marquand. Faa authorises zipline and wing for bylos operations in dallas, 2023. Accessed: 2024-10-19. URL: https://www.revolution.aero/news/2024/07/30/faa-authorises-zipline-and-wing-for-bylos-operations-in-dallas/.
- 17 Jon Ander Martin, Justin N Ouwerkerk, Anthony P Lamping, and Kelly Cohen. Comparison of battery modeling regression methods for application to unmanned aerial vehicles. *Complex Engineering Systems*, 2, 2022.
- Adnan Nuhic, Tarik Terzimehic, Thomas Soczka-Guth, Michael Buchholz, and Klaus Dietmayer. Health diagnosis and remaining useful life prognostics of lithium-ion batteries using data-driven methods. *Journal of power sources*, 239:680–688, 2013.
- Maziar Raissi, Paris Perdikaris, and George E Karniadakis. Physics-informed neural networks: A deep learning framework for solving forward and inverse problems involving nonlinear partial differential equations. *Journal of Computational physics*, 378:686–707, 2019. doi: 10.1016/J.JCP.2018.10.045.
- 20 Dapai Shi, Jingyuan Zhao, Zhenghong Wang, Heng Zhao, Chika Eze, Junbin Wang, Yubo Lian, and Andrew F Burke. Cloud-based deep learning for co-estimation of battery state of charge and state of health. *Energies*, 16(9):3855, 2023.
- 21 Guangyao Shi, Nare Karapetyan, Ahmad Bilal Asghar, Jean-Paul Reddinger, James Dotterweich, James Humann, and Pratap Tokekar. Risk-aware uav-ugv rendezvous with chance-constrained markov decision process. In 2022 IEEE 61st Conference on Decision and Control (CDC), pages 180–187. IEEE, 2022. doi:10.1109/CDC51059.2022.9993358.
- 22 Mostafa M Shibl, Loay S Ismail, and Ahmed M Massoud. A machine learning-based battery management system for state-of-charge prediction and state-of-health estimation for unmanned aerial vehicles. *Journal of Energy Storage*, 66:107380, 2023.
- Gina Sierra, M Orchard, Kai Goebel, and C Kulkarni. Battery health management for small-size rotary-wing electric unmanned aerial vehicles: An efficient approach for constrained computing platforms. *Reliability Engineering & System Safety*, 182:166–178, 2019. doi: 10.1016/J.RESS.2018.04.030.
- 24 Ellis L Thompson, Abenezer G Taye, Wei Guo, Peng Wei, Marcos Quinones, Ibrahim Ahmed, Gautam Biswas, Jesse Quattrociocchi, Steven Carr, Ufuk Topcu, et al. A survey of evtol aircraft and aam operation hazards. In AIAA AVIATION 2022 Forum, page 3539, 2022.